Physics

Physics fields

Okayama University   *Year* 2007

Phase equilibria and interfacial tension of fluids confined in narrow pores

Yoshinobu Hamada[*]   Kenichiro Koga[†]

Hideki Tanaka[‡]

[*]Okayama University

[†]Okayama University, koga@cc.okayama-u.ac.jp

[‡]Okayama University

Phase equilibria and interfacial tension of fluids confined in narrow pores

Yoshinobu Hamada, Kenichiro Koga,[a] and Hideki Tanaka
Department of Chemistry, Faculty of Science, Okayama University, 700-8530, Japan

Correlation between phase behaviors of a Lennard-Jones fluid in and outside a pore is examined over wide thermodynamic conditions by grand canonical Monte Carlo simulations. A pressure tensor component of the confined fluid, a variable controllable in simulation but usually uncontrollable in experiment, is related with the pressure of a bulk homogeneous system in equilibrium with the confined system. Effects of the pore dimensionality, size, and attractive potential on the correlations between thermodynamic properties of the confined and bulk systems are clarified. A fluid-wall interfacial tension defined as an excess grand potential is evaluated as a function of the pore size. It is found that the tension decreases linearly with the inverse of the pore diameter or width. © *2007 American Institute of Physics*. [DOI: 10.1063/1.2759926]

I. INTRODUCTION

When a fluid is confined in a nanopore, its microscopic and thermodynamic properties are determined by many factors such as pore size, geometry, atomistic details of the surfaces, etc., in addition to those determining bulk properties. There are many experimental and theoretical studies reporting that phase behavior of a fluid in such extreme confinement is qualitatively different from, and often much richer than, that of the bulk counterpart.[1–5] It is as yet difficult to predict phase behavior of a confined fluid even if the bulk phase behavior is completely known and the pore confining the fluid is fully characterized.[6,7] A main reason is that we still do not know how these fundamental characteristics of the pore alter the thermodynamic properties of the fluid. It seems essential to clarify how each of the factors affects the phase behavior of a confined fluid.

Computer simulation is a powerful tool to examine such effects on confined fluids.[8–15] In some cases, simulation reveals unexpected phase behavior of a confined fluid and then experiments confirm the results.[16,17] In molecular simulation one may deal with molecules in a portion of the pore alone, ignoring all the rest including molecules in a bulk phase in equilibrium with those in the pore, so that the computational cost is greatly reduced and thus a wider range of the thermodynamic space can be examined. A common thermodynamic condition used in molecular dynamics simulations of this kind is the one in which number of molecules N, temperature T, and pressure-tensor components, say P_{xx}, are fixed; the bulk phase pressure P_{bulk}, a constant in common experiments, is not specified. It is well recognized that T and the chemical potential μ are uniform in an entire system in equilibrium (even if the system consists of confined and bulk regions) whereas P_{xx}, etc., in a confined region are different from P_{bulk}. (Also two components, say P_{xx} and P_{yy}, are in general different unless the two directions are equivalent by the system's symmetry.) Little known is how the pressure-tensor components P_{xx}, etc., are correlated with P_{bulk} when the pore size is only a few multiples of the molecular diameter.

In this paper we report how basic characteristics of a pore, such as dimensionality, size, and pore-fluid interaction, alter the phase behavior of a confined fluid. We examine correlations between thermodynamic properties of the confined fluid and those of the bulk fluid including density-density and pressure tensor-pressure correlations. We also discuss a fluid-wall interfacial tension and its pore-size dependence, which is in turn related with the pore-size dependence of the pressure tensor component. Model systems are taken to be as simple as possible: Lennard-Jones (LJ) particles confined in either slit or cylindrical pores. The pore surface bears no atomic structure: the fluid-pore interaction is modeled by hard-sphere potentials with or without a uniform potential $\epsilon_w < 0$. More realistic models would give numerical results to be compared with experimental results of a particular system, but simple models would be more convenient for examining general properties on confined fluids, which is our concern. The equilibrium between confined and bulk regions are achieved by grand canonical Monte Carlo (GCMC) simulations.

In Sec. II we briefly describe some thermodynamic expressions for confined fluids in slit and cylindrical pores; in Sec. III we define model systems and describe simulation details; in Sec. IV we give numerical results and discussions. Summary is given in Sec. V.

II. THERMODYNAMIC EXPRESSIONS FOR CONFINED FLUIDS

When a fluid is confined between plane-parallel solid walls, its thermodynamic state may be specified by the number N of molecules, the entropy S, the total area of fluid-wall interfaces A, and the width h of the lamella. The volume of the lamella is $V = Ah/2$. Then the infinitesimal change in the internal energy U is given by[18]

[a]Author to whom correspondence should be addressed. Electronic mail: koga@cc.okayama-u.ac.jp

$$dU = TdS + \mu dN + f_{\text{pore}}dA + f_{\text{wall}}dh$$
$$= TdS + \mu dN - P_{\text{pore}}(h/2)dA - P_{\text{wall}}(A/2)dh, \qquad (1)$$

where $f_{\text{pore}} = (\partial U / \partial A)_{S,h,N}$ is a quantity with the same dimension as, but not physically identical to, the interfacial tension (f_{pore} here is γ' in Ref. [18]) and $f_{\text{wall}} = (\partial U / \partial h)_{S,A,N}$ a force acting on a wall, and

$$P_{\text{pore}} = -2f_{\text{pore}}/h, \quad P_{\text{wall}} = -2f_{\text{wall}}/A. \qquad (2)$$

Both P_{pore} and P_{wall} have a dimension of force divided by area, and the former may be considered as the pressure-tensor component parallel to the walls and the latter as that normal to the walls.

The quantities f_{pore}, f_{wall}, and P_{wall} in Eq. (1) are well defined because dU, dA, dh, and A itself are well defined (indeed there is no ambiguity in definition of A when periodic boundary conditions are introduced in directions parallel to the walls). However, the pore width h is not uniquely defined on the molecular scale but is dependent on one's choice of the positions of interfaces, and thus P_{pore} must formally be a function of h. Following the standard reference,[19] let us denote by square brackets such changes in functions that follow from a notional change in the pore size (here the width h). Then $[dP_{\text{pore}}/dh] = 2f_{\text{pore}}/h^2$.

Let the infinitesimal work $-P_{\text{pore}}(h/2)dA$ in Eq. (1) be decomposed into two contributions, one associated with the change in the fluid-wall interfacial area and one associated with the change in V under the bulk pressure,

$$-P_{\text{pore}}(h/2)dA = \gamma dA - P_{\text{bulk}}(h/2)dA.$$

This defines the fluid-wall interfacial tension γ. Then Eq. (1) is rewritten as

$$dU = TdS + \mu dN + \gamma dA - P_{\text{bulk}}(h/2)dA - P_{\text{wall}}(A/2)dh, \qquad (3)$$

where $-P_{\text{bulk}}(h/2)dA$ accounts for the work that would be done by the volume change $(h/2)dA$ on a homogeneous bulk system of the same T and μ, and γdA is the remaining contribution (to the actual work done by the volume and area changes at fixed h) that accounts for inhomogeneity in the confined system. The definition of γ is the same in spirit as Gibbs' definition of the surface tension of droplets which employs the pressure of the stable bulk phase, not the actual pressure in the droplet.[19,20] Also note that the definition of γ above Eq. (3) is in accord with that of γ in Ref. 1 but is different from γ' in Ref. 18, which is f_{pore} as remarked above. Likewise P_{bulk} is the pressure in the bulk region, a function of μ and T alone, and has no reference to the pressure tensor of the confined fluid. If we integrate Eq. (3) at fixed h, introduce the grand potential $\Omega = U - TS - \mu N$, and rewrite $hA/2$ as V, we have

$$\Omega = \gamma A - P_{\text{bulk}}V \quad \text{or} \quad \Omega^{\text{ex}} = \gamma A, \qquad (4)$$

where $\Omega^{\text{ex}} \equiv \Omega + P_{\text{bulk}}V$ the excess grand potential. If the equation above Eq. (3) (the definition of γ) is divided by dA, then we find

$$P_{\text{bulk}} - P_{\text{pore}} = \frac{2\gamma}{h} \quad \text{(slit pore).} \qquad (5)$$

The γ, too, varies not only with a physical change in h but also with the unphysical, notional change in h explained above, as P_{pore} does. From (5) we find formal dependence of the interfacial tension γ on h,

$$\left[\frac{d\gamma}{dh}\right] = \tfrac{1}{2}P_{\text{bulk}} \quad \text{or} \quad [\Delta\gamma] = \tfrac{1}{2}P_{\text{bulk}}\Delta h. \qquad (6)$$

If the definition of h is changed by 1 Å when $P_{\text{bulk}} = 1$ atm, then the interfacial tension γ is changed by $[\Delta\gamma] = 10^{-5}$ N m^{-1}. This is three orders smaller than the gas-liquid surface tension of argon at its triple point (1.3×10^{-2} N m^{-1}). So if h is defined within a reasonable range of molecular scale, and if the equilibrium bulk pressure is low, then γ would be practically independent of the definition of h.

Analogous thermodynamic relations hold for a cylindrical-pore system of length L and radius R. Again the infinitesimal change in U may be written in two ways,

$$dU = TdS + \mu dN - P_{\text{pore}}(\pi R^2)dL - P_{\text{wall}}(2\pi R)dR, \qquad (7)$$

and

$$dU = TdS + \mu dN + \gamma(2\pi R)dL - P_{\text{bulk}}(\pi R^2)dL$$
$$- P_{\text{wall}}(2\pi R)dR, \qquad (8)$$

the former defining the pressure-tensor component P_{pore} parallel to the cylindrical axis and the latter defining the fluid-wall interfacial tension γ. From Eqs. (7) and (8) one finds

$$P_{\text{bulk}} - P_{\text{pore}} = \frac{2\gamma}{R}, \qquad (9)$$

which bears an apparent resemblance to Laplace's equation. As in the case of slit-pore systems, the radius R of a cylindrical system is not uniquely defined on molecular scale: thus P_{pore} has unphysical dependence on the choice of R: $[dP_{\text{pore}}/dR] \propto 1/R^3$ and also does γ,

$$\left[\frac{d\gamma}{dR}\right] = \tfrac{1}{2}(P_{\text{bulk}} + P_{\text{pore}}) \quad \text{or}$$

$$[\Delta\gamma] = \tfrac{1}{2}\Delta R\left(P_{\text{bulk}} + \frac{P_{\text{pore}}}{1 + \Delta R/R}\right). \qquad (10)$$

III. SYSTEMS AND SIMULATION METHODS

Model systems consist of the LJ particles confined in the slit pore or in the cylindrical pore. The interaction between two particles a distance r apart is taken to be a truncated LJ 12-6 potential,

$$u(r) = \begin{cases} 4\epsilon[(\sigma/r)^{12} - (\sigma/r)^6] & (r \leq 5\sigma) \\ 0 & (r > 5\sigma). \end{cases} \qquad (11)$$

When the fluid is confined between hard walls at $z = h/2$ and $-h/2$, where the z axis is perpendicular to the walls, each particle has an additional potential independent of the x, y coordinates of its position,

$$\phi(z) = \begin{cases} \epsilon_w, & \text{if } |z| \le (h-\sigma)/2 \\ \infty, & \text{otherwise.} \end{cases} \quad (12)$$

When the fluid is confined in a hard cylindrical pore of diameter D, each particle has a potential

$$\phi(r) = \begin{cases} \epsilon_w, & \text{if } r \le (D-\sigma)/2 = R - \sigma/2 \\ \infty, & \text{otherwise,} \end{cases} \quad (13)$$

where r is the distance from the cylinder axis.

For the slit-pore system, periodic boundary conditions are imposed on two pairs of rectangular faces that are perpendicular to the walls and to each other. The simulation cell is a rectangular prism with a base of $20\sigma \times 20\sigma$ so that the total area A of fluid-wall interfaces is $2 \times (20\sigma)^2$; the distance between two walls h is set to 2, 3, 5, 11σ. Likewise, for the cylindrical-pore system, the periodic boundary condition is imposed on a pair of circular faces perpendicular to the cylinder axis. The length of the cylindrical cell is taken to be 200σ and the pore diameter D is set to 2, 3, 5, 11σ.

Equilibrium properties of the model confined fluid at fixed μ, V, and T are obtained by the standard GCMC simulation.[21] Let z be the activity of the fluid molecules, defined so as to become asymptotic to the number density $\rho = N/V$ in the limit $\rho \to 0$. Then $z/\rho = \exp[(\mu - \mu^{\text{id}})/kT]$ where μ^{id} is the ideal part of μ. It is z rather than μ that is preset in the GCMC simulation. In the numerical calculation and the analysis, all variables and results are expressed in dimensionless forms (denoted by superscript $*$) with use of the LJ energy and size parameters ϵ and σ. For example, $T^* = kT/\epsilon$, $\rho^* = \rho\sigma^3$, $z^* = z\sigma^3$, $\mu^* = \mu/\epsilon$, and $P^* = P\sigma^3/\epsilon$. We preset $\mu_c \equiv T^* \ln z^*$ and T^* in the actual calculation to obtain equilibrium properties of the confined fluid; when we wish to present these quantities as a function of μ^*, we need to specify a mass m and the LJ parameters (ϵ, σ) of a molecule and then transform z^* to μ^* by

$$\mu^* = kT^* \ln(z^* \Lambda^{*3}), \quad (14)$$

where $\Lambda^* = (h^2/2\pi mkT)^{1/2}\sigma^{-1} = (h^2/2\pi m\epsilon T^*)^{1/2}\sigma^{-1}$. In such cases the parameter set is taken to be those of argon: $m = 6.63 \times 10^{-26}$ kg, $\epsilon/k = 120$ K, and $\sigma = 3.4$ Å. Then the actual pressure P is given by $P = 42.153 P^*$ MPa.

For the corresponding bulk fluid, independent GCMC simulations are performed for the system of $V = 10\sigma \times 10\sigma \times 10\sigma$ with the same intermolecular potential (11) and with the periodic boundary conditions on each face of the cubic box. It is then confirmed that the equation of state for the LJ fluid thus obtained is in good agreement with that of the well-established empirical formula[22] with the potential cutoff correction: so we employ the empirical formula when it is more convenient.

The GCMC simulations for the bulk and confined systems are implemented as follows: first, each of the three trail actions ("move," "insert," "remove" a particle) is chosen at random with the equal probability; second, the chosen attempt is accepted or rejected according to the Boltzmann sampling algorithm;[21] and third the above procedures are repeated. We define the number of configurations generated in each simulation as the number of any trail actions. At each thermodynamic state 20×10^6 to 500×10^6 configurations

TABLE I. Conditions of the GCMC simulations of confined and bulk fluids. The interval of T^* is 0.1 and that of μ_c^* is 0.05.

System	Pore size	T^*	$\mu_c^* \equiv T^* \ln z^*$
Cylindrical	$D^* = 2$	0.6 to 1.0	−4.9 to 4.9
	3	1.0	−4.9 to 4.9
	5	0.7 to 1.0	−4.9 to 4.9
	11	0.8 to 1.2	−4.0 to 4.0
Slit	$h^* = 2$	0.7 to 1.1	−4.45 to 4.9
	3	1.0	−2.65 to 4.8
	5	0.9 to 1.3	−4.0 to 4.9
	11	0.9 to 1.2	−4.0 to 4.0
Bulk		0.8 to 1.3	−4.9 to 4.9

are generated for equilibration and 20×10^6 to 1.5×10^9 configurations are used for averaging. The number density, ρ_{pore}, of molecules in the pore is defined as the average number of molecules in the pore divided by V, the volume of pore: $\rho_{\text{pore}} = \langle N \rangle / V$: For the slit pore $V = Ah/2$ with h being the pore width in Eq. (12) and A the *total* area of the two parallel surfaces; for the cylindrical pore $V = \pi R^2 L_z$ with R the radius of pore in (13) and L_z the length of cylinder. The pressure-tensor component P_{pore} parallel to the slit-pore surfaces (the x, y plane) or parallel to the cylinder axis (the z axis) is obtained from the virial components associated with that direction,

$$P_{\text{pore}} = \begin{cases} \rho_{\text{pore}}kT + \dfrac{1}{2V}\left\langle \displaystyle\sum_{i<j}(x_{ij}f_{ij}^x + y_{ij}f_{ij}^y)\right\rangle & \text{(slit pore)} \\[3mm] \rho_{\text{pore}}kT + \dfrac{1}{V}\left\langle \displaystyle\sum_{i<j} z_{ij}f_{ij}^z\right\rangle & \text{(cylindrical pore).} \end{cases}$$

With the length of the GCMC simulations, the magnitude of statistical errors in the density and pressure are typically as follows: $\delta\rho_{\text{pore}}^*/\rho_{\text{pore}}^* \lesssim 0.002$ and $\delta P_{\text{pore}}^*/P_{\text{pore}}^* \lesssim 0.01$ for most thermodynamic conditions and $\delta\rho_{\text{pore}}^*/\rho_{\text{pore}}^* \lesssim 0.006$ and $\delta P_{\text{pore}}^*/P_{\text{pore}}^* \simeq 0.1$ for exceptional cases where the density is extremely low or high, where δ is the difference in the quantity between two independent GCMC simulations with the equal length. Use of the standard GCMC sampling suffices for the present study as long as the system remains in a disordered liquid-like state, which is indeed confirmed by many ways such as comparison with the empirical equation of state, comparison with a different sampling method, magnitudes of error bars, and consistency (no scattering) of a series of data points; when the system turns into a solid state the standard method cannot give accurate results as expected and should be replaced by some non-Boltzmann sampling method, but the focus of the present study is on the properties of the confined *fluids*, so the standard sampling method suffices for our purpose. Simulation details are summarized in Table I.

The grand-canonical partition function $\Xi(\mu, T; \epsilon_w)$ of a fluid in a hard pore with a uniform potential ϵ_w is mapped to that of the fluid in the hard pore with a different uniform potential ϵ_w' at different chemical potential μ'. Let H and H'

be the Hamiltonian of a system of N molecules with uniform potentials ϵ_w and ϵ'_w. Since they are related by $H - N\epsilon_w = H' - N\epsilon'_w$,

$$\Xi(\mu, T; \epsilon_w) = \sum e^{\mu N/kT} e^{-H/kT} \tag{15}$$

$$= \sum e^{(\mu - \epsilon_w + \epsilon'_w)N/kT} \sum e^{-H'/kT}. \tag{16}$$

That is,

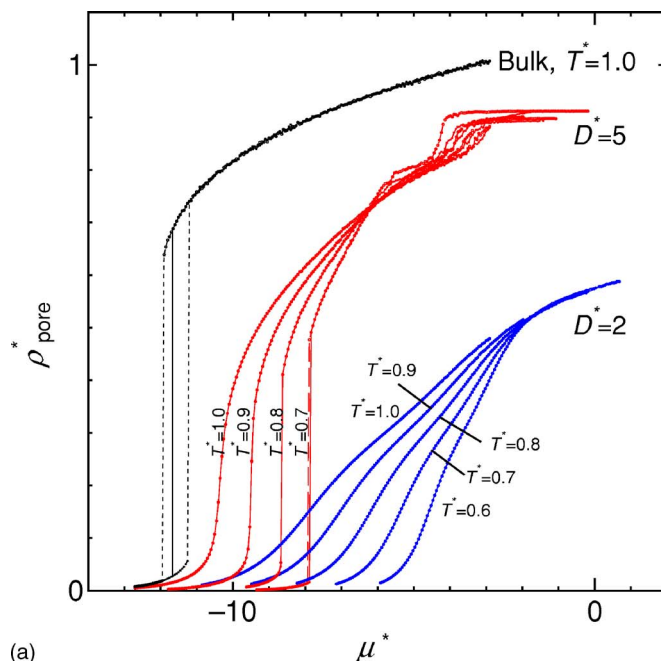$$\Xi(\mu, T; \epsilon_w) = \Xi(\mu', T; \epsilon'_w), \quad \mu' = \mu - \epsilon_w + \epsilon'_w. \tag{17}$$

Setting $\epsilon'_w = 0$, in particular, one finds that a partition function for the hard-wall pore with any given ϵ_w is mapped to the one with no attractive potential. We make full use of this fact in examining the effect of the fluid-wall attractive potential ϵ_w on the phase equilibria between the bulk and confined fluids.

IV. NUMERICAL RESULTS AND ANALYSIS

A. Pore-size and pore-dimensionality effects on the phase behavior

We first illustrate pore-size effects on the phase behavior of the simple fluid in hard cylindrical or slit pore (Figs. 1 and 2). The GCMC simulation of the confined fluids gives the equilibrium ρ^*_{pore}, P^*_{pore}, etc., for each thermodynamic state specified by preset values of μ^*, T^*, and D^* (or h^*). The formulas for P^*_{pore} and ρ^*_{pore} are given in Sec. III. Figure 1(a) shows the density ρ^*_{pore} of the cylindrically confined fluid as a function of μ^* at fixed T^*. Structural changes detected by the density profiles, the radial distribution function, and three dimensional structures as well as changes in the density and potential energy indicate that the confined fluids at $D^* = 2$ and 5 undergo gas-liquid and liquid-solid phase changes in the ranges of μ^* examined, but the type of phase changes depends on T^* and D^*. At $D^* = 2$, both the gas-liquid and liquid-solid phase changes are continuous with no hysteresis for $T^* = 0.6$ (lower than the triple point $T^*_{tp} \simeq 0.69$ of the bulk fluid) and above: a liquid-solid phase change being continuous is only possible in one-dimensional systems. At $D^* = 5$, however, the liquid-solid phase change is discontinuous for any fixed values of T^* while the gas-liquid phase change is continuous with no hysteresis when $T^* \geqslant 0.8$. The bulk fluid at $T^* = 1.0$ undergoes a gas-liquid first-order phase transition with a large hysteresis loop.

When a phase change is accompanied by a hysteresis loop, the phase equilibrium point is not determined from an isotherm in a density-field plane (e.g., the ρ_{pore}-μ isotherm) but is determined from an isotherm in a field-field plane. This is because at a first-order transition the latter isotherm is always continuous and its slope is discontinuous, and so such a point is unambiguously identified even if the system exhibits hysteresis. Plotted in Fig. 1(b) are the $\ln P^*_{pore}$-μ^*/T^* isotherms for the same systems as in Fig. 1(a). Discontinuous change in slope is found for $D^* = 5$ and the bulk system. Two branches of the bulk-system isotherm intersect at $\mu^* \simeq -11.7$ when $T^* = 1.0$, which is a gas-liquid phase equilibrium point [shown as a vertical line in Fig. 1(a)]. The isotherms
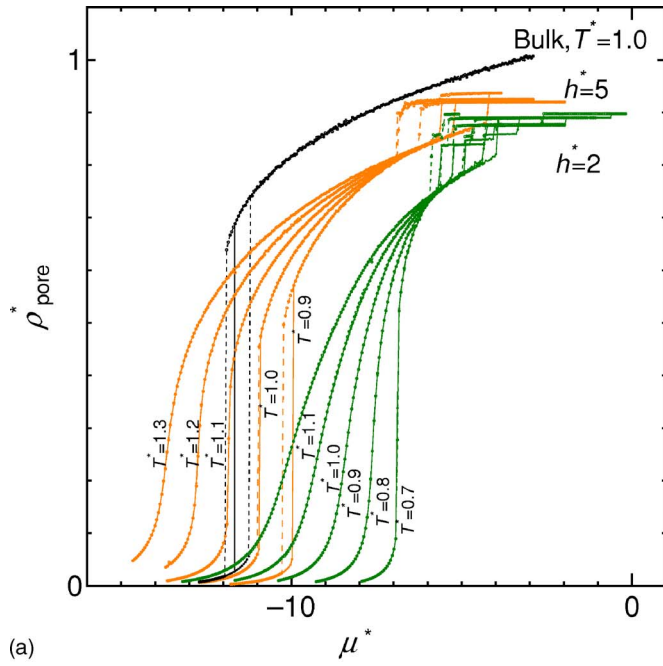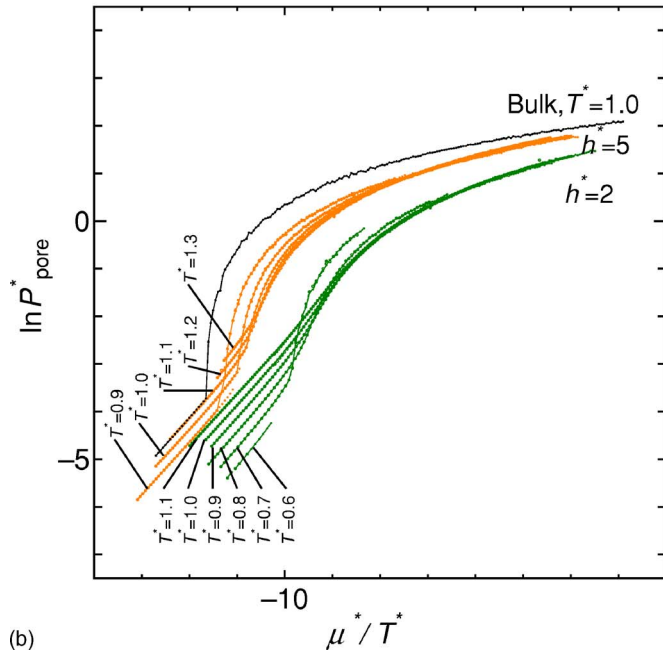

FIG. 1. (a) ρ^*_{pore}-μ^* and (b) $\ln P^*_{pore}$-μ^*/T^* isotherms of the LJ fluids in the cylindrical pores. Dashed curves in (a) indicate hysteresis.

for the system of $D^* = 2$ are smooth for the entire range of μ^*/T^*, indicating nonexistence of first-order phase transitions in this pore.

For the slit-pore systems, liquid-solid phase changes observed are all discontinuous in contrast to the cylindrical-pore systems, as seen from the isotherms in Fig. 2. Gas-liquid phase change in the pore of width $h^* = 5$ is continuous when $T^* \geqslant 1.1$ and the one for $h^* = 2$ is continuous when $T^* \geqslant 0.8$. The lowest temperature for the continuous phase change being possible is the gas-liquid critical temperature T_c. In practice, the critical temperature was determined as a temperature whose isotherm [in Figs. 1(a) and 2(a)] exhibits a continuous phase transition and the isotherm just below

(a)

(b)

FIG. 2. (a) $\rho^*_{pore} - \mu^*$ and (b) $\ln P^*_{pore} - \mu^*/T^*$ isotherms of the LJ fluids in the slit pores. Dashed curves in (a) indicate hysteresis.

with decreasing pore size: such decrease in cohesive energy in turn reduces the gas-liquid surface tension and thereby lowers the T_c. The same explanation applies to the effect of the pore dimensionality: the T_c is lower for the cylindrical pore than for the slit pore. We will also examine how fluid-pore attractive interaction alters the above pictures.

It should be noted that although the liquid-solid phase transitions are evident in the discontinuous changes in ρ^* in Figs. 1(a) and 2(a), it is difficult to achieve equilibrium states of solid phases in the GCMC simulation: results involving solid phases are not shown in Figs. 1(b) and 2(b).

Irrespective of temperature, pore size, pore dimensionality, the slope of $\ln P^*_{pore}$-μ^*/T^* isotherm goes to 1 as ρ^* goes to zero [see Figs. 1(b) and 2(b)], as required for the ideal gas. In the same limit the ideal gas law $P^*_{pore} = \rho^*_{pore} T^*$ is confirmed, provided that both P^*_{pore} and ρ^*_{pore} are defined with a common diameter or width, which is now chosen to be h in Eq. (12) or D in Eq. (13) but is not necessarily so.
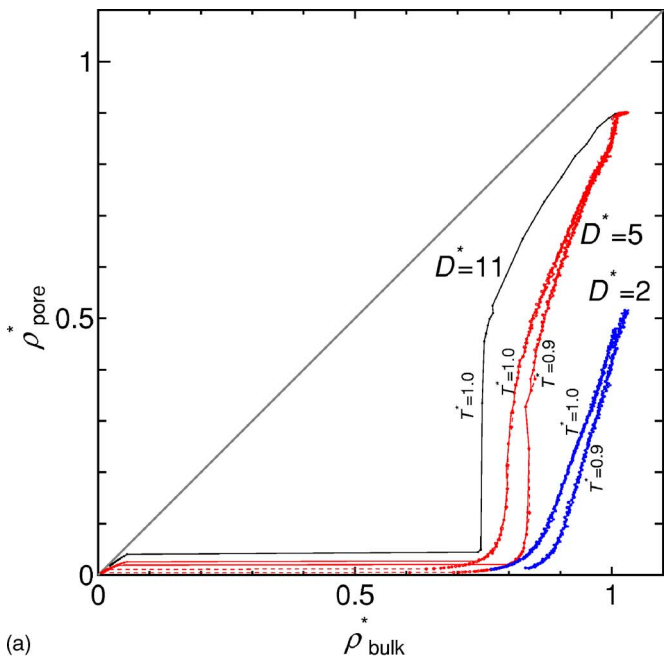
B. Correlation between confined and bulk phase behaviors

We have seen that the larger the pore size D or h the lower the μ (or P_{bulk}) at which the confined liquid evaporates (and the bulk liquid evaporates at the lowest μ). We shall now examine how such shift in two-phase equilibrium manifests itself in the density-density (ρ_{pore}-ρ_{bulk}) and the pressure-pressure (P_{pore}-P_{bulk}) correlations between the pore and the bulk regions.
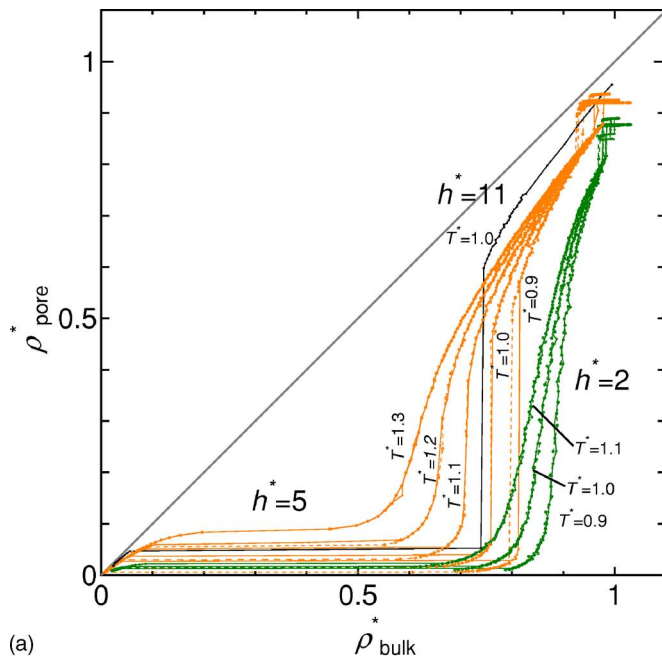
Plotted in Fig. 3 are (ρ_{pore}, ρ_{bulk}) and (P_{pore}, P_{bulk}) isotherms for the cylindrical pores. The ρ_{pore}-ρ_{bulk} plot in Fig. 3(a) shows large deviation from the linear relation $\rho_{pore} = \rho_{bulk}$: a horizontal part and a vertical or steep angle part in each curve correspond to the gas-liquid transitions in the bulk and confined systems, respectively. As the pore diameter D becomes larger, or T is increased, the deviation of the ρ_{pore}-ρ_{bulk} curve from $\rho_{pore} = \rho_{bulk}$ becomes less pronounced. But, the horizontal and vertical parts would never disappear so long as D remains finite: they disappear only when the gas-liquid transitions in the two systems occur at exactly the same μ at given T since ρ_{pore} or ρ_{bulk} is discontinuous at the first-order transition. The pressure is, however, continuous at the transition. So the P_{pore}-P_{bulk} plot should approach $P_{pore} = P_{bulk}$ continuously with increasing D, which is shown in Fig. 3(b).

As shown in the inset of Fig. 3(b), with increasing P_{bulk}, first the slope dP_{pore}/dP_{bulk} is close to 1 when the fluid is in a gaseous state both in the confined and bulk regions; second it becomes much smaller than 1 when the fluid remains in a gaseous state in the pore but it is in a liquid state in the coexisting bulk system; and finally the slope gets steeper abruptly ($D^* = 11$) or gradually ($D^* = 2, 5$) when the gas-liquid condensation takes place in the pore.
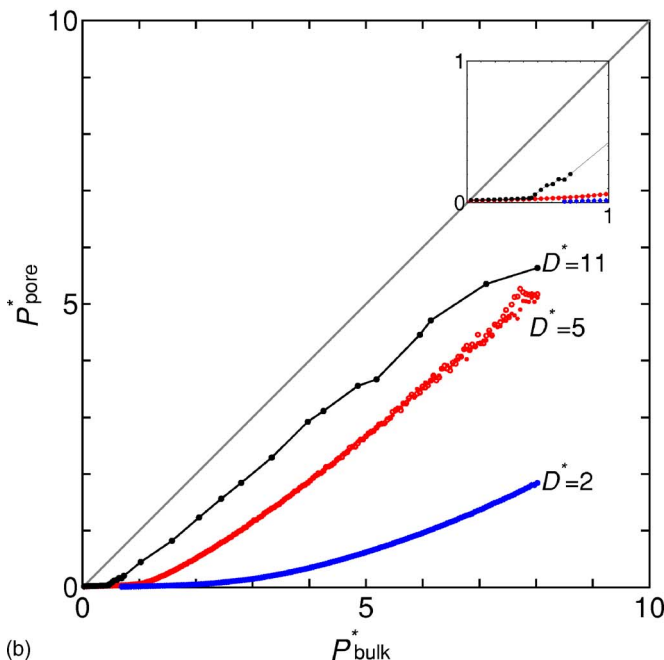
In Fig. 4 are shown the ρ_{pore}-ρ_{bulk} and P_{pore}-P_{bulk} plots for the slit-pore systems. They are qualitatively similar to those for the cylindrical-pore systems. It is noted that deviation of the P_{pore}-P_{bulk} curve from the linear $P_{pore} = P_{bulk}$ is

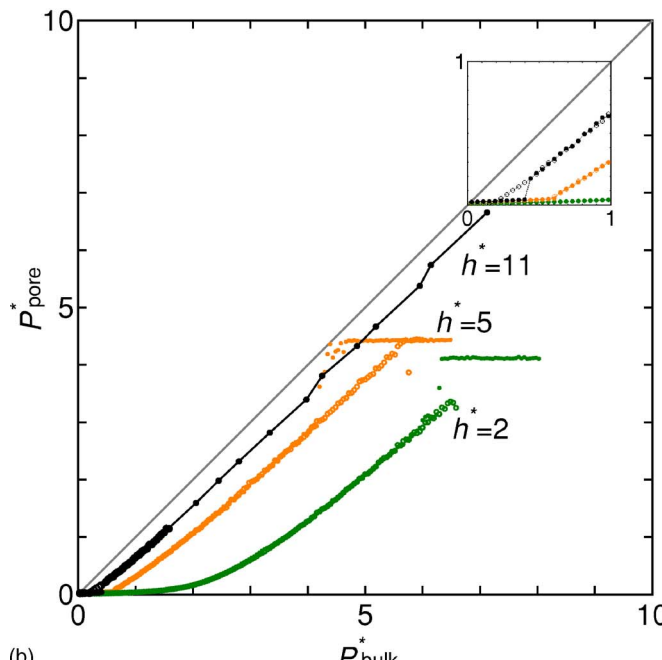that temperature by 0.1 in the reduced unit exhibits a discontinuous phase transition. The critical pressure tensor $P_{c,pore}$ was then identified with the pressure tensor at the inflection point in the isotherm of T_c. Our results illustrate that T_c is higher for the slit-pore system than for the cylindrical-pore system if $h = D$. Also it is clear from Figs. 1 and 2 that the smaller the pore size the lower the T_c and the critical pressure tensor $P_{c,pore}$. This effect has been known[2] and may be explained intuitively as follows. The potential energy for a simple fluid confined in a purely repulsive pore would increase with decreasing the pore size because molecules in contact with such walls have higher potential energy than other molecules and the ratio of such molecules increases

FIG. 3. (a) $\rho_{pore}^* - \rho_{bulk}^*$ and (b) $P_{pore}^* - P_{bulk}^*$ isotherms of the LJ fluids in the cylindrical pores. Dashed curves in (a) indicate hysteresis.

FIG. 4. (a) $\rho_{pore}^* - \rho_{bulk}^*$ and (b) $P_{pore}^* - P_{bulk}^*$ isotherms of the LJ fluids in the slit pores. Dashed curves in (a) indicate hysteresis.

smaller for the slit-pore (quasi-two-dimensional) system than for the cylindrical-pore (quasi-one-dimensional) system provided that $h = D$.

Slope of the (P_{pore}, P_{bulk}) isotherm has a simple physical meaning,

$$\frac{dP_{pore}}{dP_{bulk}} = \frac{\rho_{pore}}{\rho_{bulk}}. \tag{18}$$

This explains that the slope is very small when the fluid is gaseous in the pore while it is liquid-like in the bulk ($\rho_{pore} \ll \rho_{bulk}$). Figures 3(b) and 4(b) show that $dP_{pore}/dP_{bulk} < 1$ when both confined and bulk fluids are liquidlike. This means that the liquid density in the pore is less than that in

the bulk, which is directly confirmed by the plots in Figs. 3(a) and 4(a).

We also note that the P_{pore}-P_{bulk} correlation for a given pore is only weakly dependent on temperature. The ρ_{pore}-ρ_{bulk} curves for different temperatures are clearly distinguishable [Figs. 3(a) and 4(a)] whereas the corresponding P_{pore}-P_{bulk} curves are almost indistinguishable [so only the curves for $T^* = 1.0$ were plotted in Fig. 3(b) and 4(b)].

C. Effect of fluid-pore attractive interaction

We have so far examined effects of pure confinement on the phase behavior by assuming the fluid-pore interaction to

be nonattractive (and infinitely hard). We now introduce a uniform potential $\epsilon_w < 0$ to the otherwise infinitely hard pore, so that the fluid-pore interaction be attractive. As described in Sec. II, the grand-canonical partition function for such a system is mapped to the partition function for the original nonattractive pore system. As for any real pore having a nonuniform continuous potential field, it is reasonable to speculate that phase equilibrium between confined and bulk regions is primarily determined by a purely geometric constraint plus a uniform mean-field corresponding to the fluid-pore attractive interaction averaged over inner space of the real pore while the nonuniform part may play some secondary role.

Figure 5 shows ρ_{pore}-ρ_{bulk} and P_{pore}-P_{bulk} correlations for the cylindrical pore ($D^* = 5$) with three different uniform potentials: $\epsilon_w^* = -0.832, -2.532, -4.232$. The first corresponds to a potential of an argon atom at the center of a single walled carbon nanotube with the same diameter;[13] the second and the third correspond to about $1/4$ and $2/5$ of the depth of the potential well for the same integrated LJ force field. Figure 5(a) illustrates that none of the ρ_{pore}-ρ_{bulk} curves is close to the linear relation $\rho_{pore}(\mu) = \rho_{bulk}(\mu)$ and that the density-density correlation is very sensitive to the fluid-pore interaction. Even for the smallest ϵ_w, with increasing μ or P_{bulk} an onset of the gas-to-liquid phase change appears in the pore and then, during the continuous change in the pore, the coexisting bulk system undergoes a gas-to-liquid discontinuous transition. The lower the pore-fluid potential ϵ_w, the higher the density ρ_{pore} in the pore when the bulk fluid undergoes the gas-to-liquid transition. But an inequality $\rho_{pore} < \rho_{bulk}$ holds for all the cases after the bulk system underwent the transition.

Figure 5(b) shows the pressure-pressure correlation for the same system as in Fig. 5(a). Unlike the density-density correlation, basic shape of the P_{pore}-P_{bulk} curve is not drastically changed with varying ϵ_w: each curve is nearly parallel to the line $P_{pore} = P_{bulk}$ and, with increasing $|\epsilon_w|$, its location is displaced from the region of $P_{pore} < P_{bulk}$ to that of $P_{pore} > P_{bulk}$. The only qualitative change is found in its initial slope near $P_{bulk}^* = 0$: it is close to zero for $\epsilon_w^* = 0$ and -0.832 whereas it is nearly vertical for $\epsilon_w^* = -2.532$ and -4.232. This difference reflects whether or not the gas-liquid transition in the pore precedes that in the bulk as P_{bulk} increases at constant T.

It is worth noting that when $\epsilon_w^* = -2.532$, the P_{pore}-P_{bulk} correlation is very close to the identity $P_{pore} = P_{bulk}$ for $P_{bulk}^* > 2$. Since this value for ϵ_w is in the range between the local maximum and minimum of the argon-nanotube potential, it is possible for a real system to have such pressure-pressure relation for an extended range of P_{bulk}.

The ρ_{pore}-ρ_{bulk} and P_{pore}-P_{bulk} correlations for the slit-pore system are qualitatively similar to those for the cylindrical-pore system (Fig. 6). To make contact with a real system, as we did for the cylindrical pore, we now refer to a LJ 9-3 potential for water between two hydrocarbon walls[23] placed at $z = \pm 3\sigma$ (where the potential becomes ∞). Then $\epsilon_w^* = -0.1438$ and -1.955 (those scaled by the LJ energy parameter ϵ for the fluid-fluid interaction) correspond to the potentials at $z = 0$ (the midpoint) and at a distance 3.46 Å
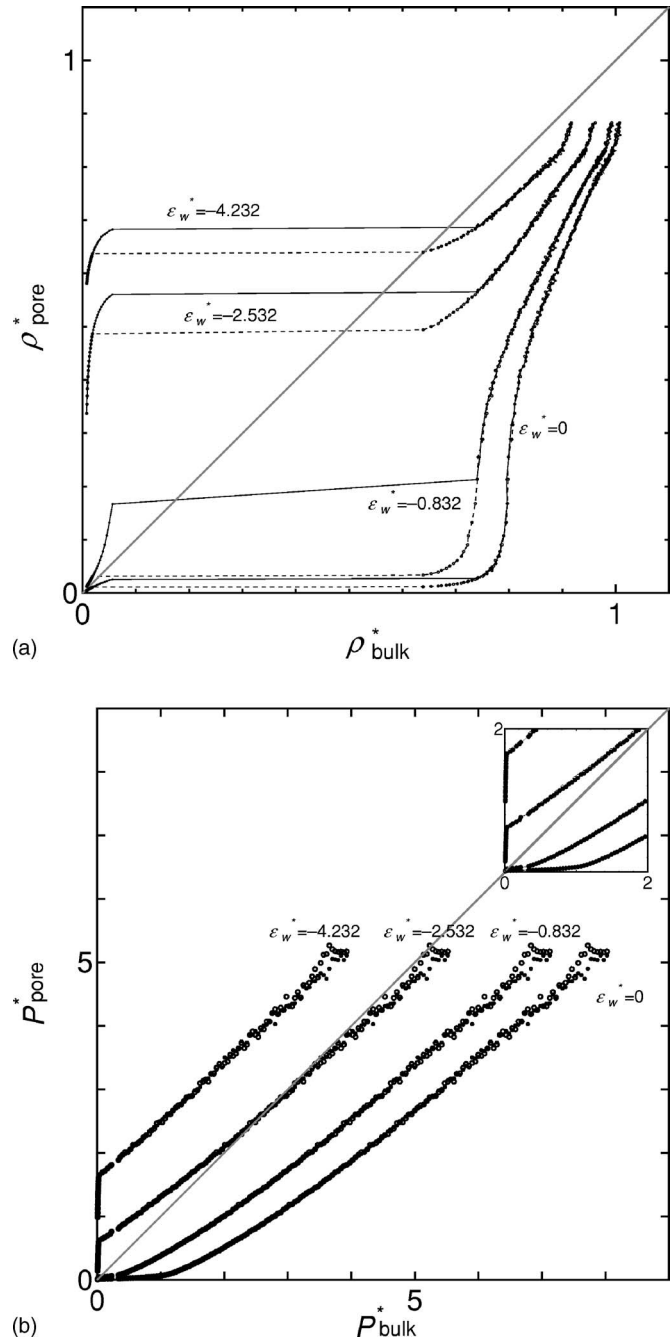

FIG. 5. (a) ρ_{pore}^*–ρ_{bulk}^* and (b) P_{pore}^*–P_{bulk}^* isotherms of the LJ fluids in the attractive cylindrical pores of $D^* = 5$ at $T^* = 1.0$. Dashed curves in (a) indicate hysteresis.

apart from each wall. As shown in Fig. 6(a), for slit pores with $\epsilon_w^* \geq -0.1438$, the condensation succeeds that in the bulk as μ increases (and so does P_{bulk}) whereas for pores with $\epsilon_w^* \leq -1.0494$ it precedes that in the bulk. This is also shown in the inset of Fig. 6(b). When both the confined and bulk fluids are in liquid states, the density in the pore is always lower than the bulk-fluid density. Discontinuities in ρ_{pore} at about $\rho_{bulk}^* = 0.9$ are manifestations of freezing in the confined liquid. The P_{pore}-P_{bulk} curves are near linear for all the cases of ϵ_w and the one for $\epsilon_w^* = -1.0494$ is the closest to the special line $P_{pore} = P_{bulk}$. In passing we note that there are ranges in which P_{pore} is nearly constant with respect to P_{bulk}: what happened there is that the system underwent a liquid-
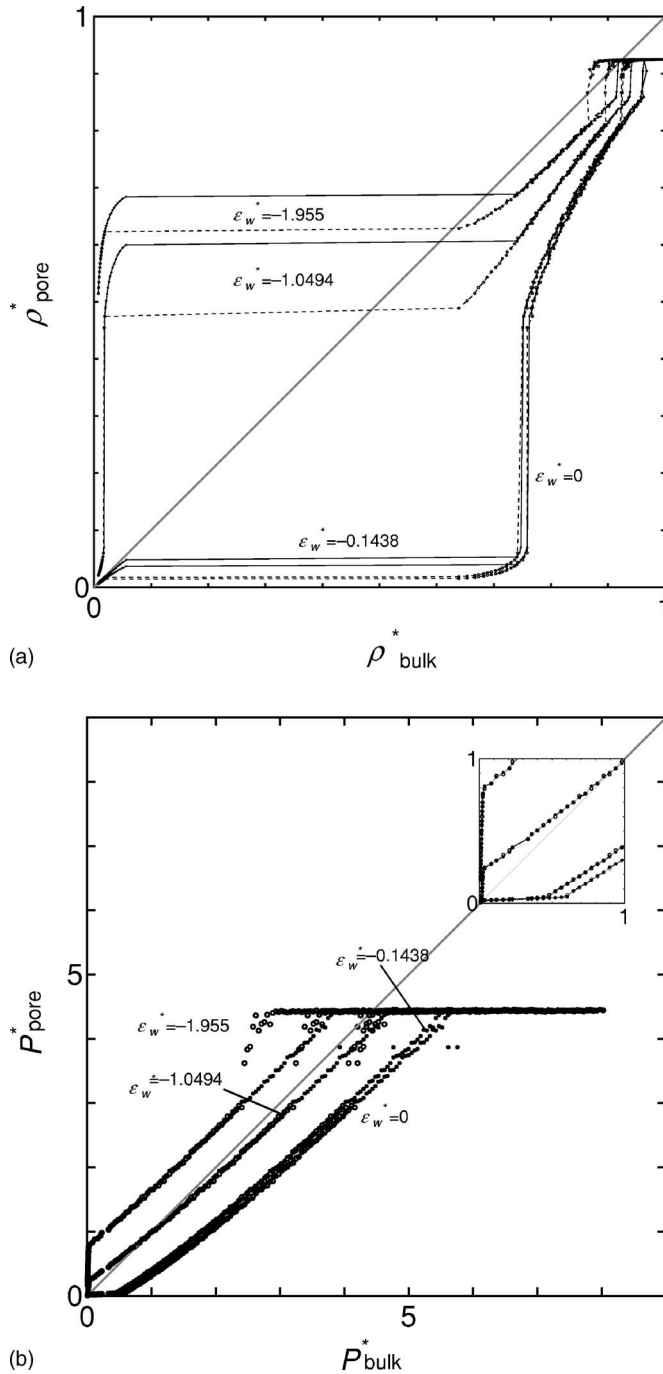
(a)

ρ^*_{pore}

$\varepsilon^*_w = -1.955$

$\varepsilon^*_w = -1.0494$

$\varepsilon^*_w = 0$

$\varepsilon^*_w = -0.1438$

ρ^*_{bulk}

(b)

P^*_{pore}

$\varepsilon^*_w = -0.1438$

$\varepsilon^*_w = -1.955$

$\varepsilon^*_w = -1.0494$

$\varepsilon^*_w = 0$

P^*_{bulk}

FIG. 6. (a) $\rho^*_{\text{pore}} - \rho^*_{\text{bulk}}$ and (b) $P^*_{\text{pore}} - P^*_{\text{bulk}}$ isotherms of the LJ fluids in the attractive slit pores of $h^* = 5$ at $T^* = 1.0$. Dashed curves in (a) indicate hysteresis.

to-solid transition and the equilibrium P_{pore} and ρ_{pore} were not achieved for the solid states in the GCMC simulation.

D. Effect of the pore size on the interfacial tension

The interfacial tension γ defined in Sec. II is given in terms of the difference $P_{\text{bulk}} - P_{\text{pore}}$ and the pore size h or R, which are directly accessible or preset in the GCMC simulation. Here we focus on the effect of pore size on γ for fixed bulk pressures ($P^*_{\text{bulk}} = 1.0, 2.1, 2.8, 4.0, 4.9, 6.0$) and a fixed temperature ($T^* = 1.0$). Under the thermodynamic conditions, neither bulk nor confined system is in a gaseous state. In
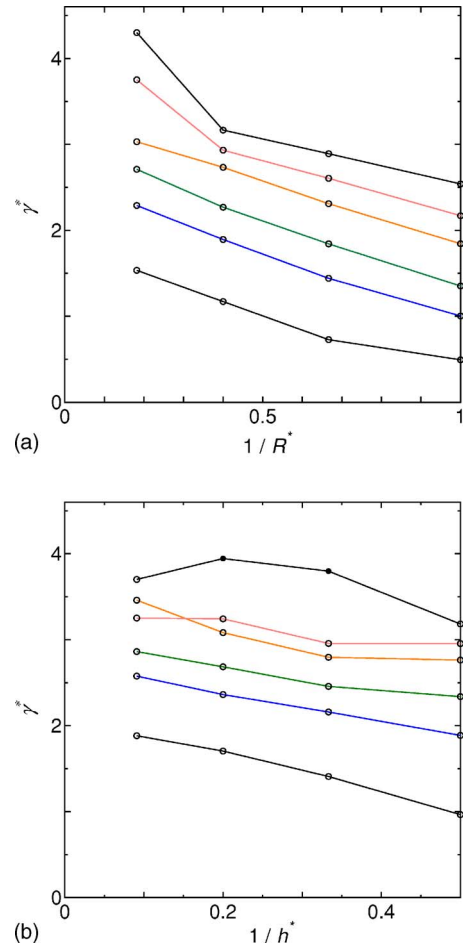

(a)

γ^*

$1 / R^*$

(b)

γ^*

$1 / h^*$

FIG. 7. Fluid-wall interfacial tension γ^* as a function of the inverse of the pore size $1/R^*$ or $1/h^*$: (a) cylindrical-pore systems and (b) slit-pore systems; for all the cases, the pore-fluid attractive interaction $\epsilon^*_w = 0$, $T^* = 1.0$; the bulk pressure is fixed at $P^*_{\text{pore}} = 1.004, 2.063, 2.829, 4.025, 4.918, 6.021$ from the bottom to top curves.

order to achieve greater precision, we have evaluated P_{bulk} at any given μ from the empirical equation of state for the LJ fluid[22] considering the potential cutoff. Essentially the same numerical results are obtained if we employ a polynomial fit to the values for P_{bulk} directly obtained from our GCMC simulations.

For the LJ fluid confined in the cylindrical hard pore with $\epsilon^*_w = 0$, as shown in Fig. 7(a), one finds (i) γ is always positive, (ii) γ decreases monotonically as the pore diameter D decreases, and, (iii) in particular, when fixed P^*_{bulk} is in a range between 1 and 4, one finds

$$\gamma \simeq \gamma_{\text{cyl.},\infty} - \frac{c}{R}, \tag{19}$$

where c is a positive constant and $\gamma_{\text{cyl.},\infty}$ is the fluid-wall interfacial tension in the limit $R \to \infty$, i.e., the tension between the fluid and the flat wall. This approximate pore-size dependence (19) of γ in turn suggests the dependence of P_{pore} as

$$P_{\text{pore}} = P_{\text{bulk}} - \frac{2\gamma_{\text{cyl.},\infty}}{R} + \frac{2c}{R^2}. \tag{20}$$

Figure 7(b) shows the corresponding plots for the slit-pore systems with $\epsilon_w^* = 0$. As in the cylindrical-pore systems, one finds that γ is always positive and decreases with decreasing h (except for $P_{\text{bulk}}^* = 6.0$): when $P_{\text{bulk}}^* < 3$, in particular,

$$\gamma \simeq \gamma_{\text{slit},\infty} - \frac{c_1}{h}, \tag{21}$$

where c_1 is a positive constant and $\gamma_{\text{slit},\infty}$ is the interfacial tension in the limit $h \rightarrow \infty$.

For the fixed bulk pressures at which both (19) and (21) holds, one finds numerically $\gamma_{\text{cyl},\infty} \simeq \gamma_{\text{slit},\infty}$ as it should be: when R and h go to infinity these fluid-wall interfaces become the one between the fluid and a single flat wall at given P_{bulk}, and so $\gamma_{\text{cyl},\infty} = \gamma_{\text{slit},\infty} = \gamma_\infty$. In fact, this is a useful check on the numerical results: one finds that numerical errors in γ are greater when $P_{\text{bulk}}^* > 3$ because γ's for the cylindrical and slit pores do not converge in the limits of infinitely large pores. Thus it is uncertain whether or not the pore-size dependence of γ at the higher pressures is still linear with the inverse of the pore size. We note in passing that when $P_{\text{bulk}}^* = 6.0$ the slit-pore systems with $h^* = 3$ and 5 are in solid-like states. This might be the reason for the exceptional behavior of γ at this P_{bulk}: it does *not* monotonically decreases as h.

V. SUMMARY

Phase behavior and thermodynamic properties including a pressure tensor component and a fluid-wall interfacial tension of the LJ fluid confined in cylindrical and slit pores were examined by GCMC simulation. Effects of the pore dimensionality, size, and attractive potential were studied in a systematic way.

Slope of the pressure tensor-pressure P_{pore}-P_{bulk} isotherm is close to 1 except when the confined or bulk system undergoes a phase transition. Its location is sensitive to strength of the fluid-pore attractive interaction. When the uniform potential ϵ_w is chosen to be somewhere between the local minimum and maximum of the more realistic potential model for argon in a carbon nanotube or water between graphene sheets, the P_{pore}-P_{bulk} isotherm can be very close to the identical relation P_{pore}-P_{bulk} in a wide range of the chemical potential.

A fluid-wall interfacial tension may be defined as an excess grand potential of a confined fluid over a homogeneous bulk fluid with the same T and μ. The interfacial tension so defined is dependent on the choice of the position of the dividing surface but when the bulk pressure is sufficiently low and the range of the choice is of a molecular scale the dependence would be negligible. It was found that both for the cylindrical and slit pore with no attractive potential the fluid-wall interfacial tension decreases linearly with the inverse of the pore size.

[1] R. Evans and U. Marini Bettolo Marconi, J. Chem. Phys. **86**, 7138 (1987).
[2] R. Evans, J. Phys.: Condens. Matter **2**, 8989 (1990).
[3] L. D. Gelb, K. E. Gubbins, R. Radhakrishnan, and M. Sliwinska-Bartkowiak, Rep. Prog. Phys. **62**, 1573 (1999).
[4] H. K. Christenson, J. Phys.: Condens. Matter **13**, R95 (2001).
[5] C. Alba-Simionesco, B. Coasne, G. Dosseh, G. Dudziak, K. E. Gubbins, R. Radhakrishnan, and M. Sliwinska-Bartkowiak, J. Phys.: Condens. Matter **18**, R15 (2006).
[6] T. Ohkubo, T. Iiyama, K. Nishikawa, T. Suzuki, and K. Kaneko, J. Phys. Chem. B **103**, 1859 (1999).
[7] T. Ohba, T. Omori, H. Kanoh, and K. Kaneko, J. Phys. Chem. B **108**, 27 (2004).
[8] K. Koga, X. C. Zeng, and H. Tanaka, Phys. Rev. Lett. **79**, 5262 (1997).
[9] K. Koga, H. Tanaka, and X. C. Zeng, Nature (London) **408**, 564 (2000).
[10] B. Coasne and R. J. M. Pellenq, J. Chem. Phys. **120**, 2913 (2004).
[11] A. Striolo, A. A. Chialvo, K. E. Gubbins, and P. T. Cummings, J. Chem. Phys. **122**, 234712 (2005).
[12] K. Koga and H. Tanaka, J. Chem. Phys. **122**, 104711 (2005).
[13] K. Koga and H. Tanaka, J. Chem. Phys. **124**, 131103 (2006).
[14] B. Coasne, S. K. Jain, and K. E. Gubbins, Phys. Rev. Lett. **97**, 105702 (2006).
[15] J. K. Singh and S. K. Kwak, J. Chem. Phys. **126**, 024702 (2007).
[16] K. Koga, G. T. Gao, H. Tanaka, and X. C. Zeng, Nature (London) **412**, 802 (2001).
[17] Y. Maniwa, H. Kataura, M. Abe, S. Suzuki, Y. Achiba, H. Kira, and K. Matsuda, J. Phys. Soc. Jpn. **71**, 2863 (2002).
[18] D. J. Diestler, M. Schoen, J. E. Curry, and J. H. Cushman, J. Chem. Phys. **100**, 9140 (1994).
[19] J. S. Rowlinson and B. Widom, *Molecular Theory of Capillarity* (Clarendon, Oxford, 1982).
[20] J. W. Gibbs, *The Collected Works of J. Willard Gibbs* (Longmans, Green, 1928), Vol. 1.
[21] J. Yao, R. A. Greenkorn, and K. C. Chao, Mol. Phys. **46**, 587 (1982).
[22] J. J. Nicolas, K. E. Gubbins, W. B. Streett, and D. J. Tildesley, Mol. Phys. **37**, 1429 (1979).
[23] C. Y. Lee, J. A. McCammon, and P. J. Rossky, J. Chem. Phys. **80**, 4448 (1984).